Numerical Heat Transfer, Part A, 57: 709–729, 2010

ISSN: 1040-7782 print/1521-0634 online
DOI: 10.1080/10407781003800714

Taylor & Francis
Taylor & Francis Group

MIXED CONVECTION IN AN OBSTRUCTED OPEN-ENDED CAVITY

Wenlu Shi and Kambiz Vafai

Department of Mechanical Engineering, University of California, Riverside, Riverside, California, USA

Mixed convection in an obstructed cavity with heated horizontal walls is investigated in this work. Brinkman-Forchheimer-extended Darcy model is utilized to describe the flow characteristics within a porous medium for different angles of attack with respect to the forced convection. Numerical results are obtained for a wide range of Grashof numbers (10^2–10^9), Reynolds numbers (10^2–10^5), Darcy numbers (10^{-6}–10^{-1}), and aspect ratios (0.25–2). Effects of the pertinent physical parameters are investigated in terms of the flow and temperature fields, as well as Nusselt number distributions. The presented results show that the Darcy number plays a significant role on the flow and thermal fields and the Nusselt number distributions for different flow configurations. For an inclined flow, the vertical velocity component is substantially diminished within a narrow entrance section near the inlet boundary. It is shown that as the aspect ratio increases the thickness of the thermal boundary layer increases, resulting in a decrease in the heat transfer rate though the horizontal walls.

1. INTRODUCTION

Mixed-convection heat transfer in an open-ended enclosure has received increased attention by many researchers in recent years due to its significance in various practical applications, such as cooling and drying processes, thermal insulation engineering, thermal storage systems, and underground spreading of chemical waste. Furthermore, this type of configuration, illustrates the fundamentals of interactions between inner and outer flow fields that are present in various applications. Doria [1] conducted a study of two-dimensional unsteady flow of multi-component gases incorporating buoyancy effects. In their work, a model was set up to study fire in a room. Jacobs et al. [2, 3] conducted a numerical study of steady state natural convection in open rectangular cavities. Penot [4] conducted a numerical study of free convection flow inside an isothermal open square cavity. The effects of cavity inclination and Grashof number were examined in this work. LeQuere et al. [5] used primitive variables to study the same configuration. Their results show that the unsteadiness takes place for Grashof numbers larger than 10^6. They also demonstrated the effect of the Grashof number and cavity aspect ratio and inclination.

Received 10 January 2010; accepted 12 March 2010.

Address correspondence to Kambiz Vafai, Department of Mechanical Engineering, University of California, Riverside, A363 Bourns Hall, Riverside, CA 92521-0425, USA. E-mail: vafai@engr.ucr.edu

NOMENCLATURE

A	aspect ratio of the enclosure ($A = w/H$)	u	velocity in the x-direction, $m\,s^{-1}$
Da	Darcy number	v	velocity in the y-direction, $m\,s^{-1}$
F	inertial coefficient, an empirical function that depends on the Reynolds number and the microstructure of the porous medium	U_o	external flow velocity, $m\,s^{-1}$
		U	dimensionless velocity in the x-direction
		V	dimensionless velocity in the y-direction
g	gravitational acceleration, m^2/s	w	width of the enclosure, m
Gr	Grashof number	x, y	Cartesian coordinates, m
H	height of the enclosure, m	α	thermal diffusivity, $m^2\,s^{-1}$
K	permeability of the porous medium, m^2	β	coefficient of volume expansion, K^{-1}
L_x	extended computational domain length in x-direction, m	δ	porosity
		θ	dimensionless temperature
L_y	extended computational domain length in y-direction, m	Φ	inclination angle
		μ	dynamic viscosity, $kg\,m^{-1}\,s^{-1}$
n	outward normal to a surface	ν	kinematic viscosity, $m^2\,s^{-1}$
Nu	Nusselt number	ρ	density, $kg\,m^{-3}$
p	pressure, Pa	τ	dimensionless time
P	dimensionless pressure	**Subscripts**	
Pr	Prandtl number	∞	condition at infinity
Re	Reynolds number	w	wall of the enclosure
t	time, s	f	refers to the fluid
T	temperature, C^o	e	refers to effective properties
T_w	enclosure wall temperature, C^o		

A numerical study of natural convection in a square open cavity with a heated vertical wall and two horizontal walls which are insulated was performed by Chan and Tien [6]. In this work, a wide range of Grashof numbers were investigated (10^3 to 10^9). Their results illustrated the effect of the boundary conditions on the near field and the solution close to the opening. Later on, the same authors [7] conducted a numerical study of laminar, steady-state natural convection in a two-dimensional shallow rectangular open enclosure. The flow characteristics were explored up to a Rayleigh number of 10^6. Mhiri et al. [8] conducted a numerical study of the thermal insulation in a cavity with a vertical downstream air jet using a finite volume method. Besbes et al. [9] conducted a numerical study of a heated two-dimensional cavity where the lower horizontal wall is isothermal and the two vertical walls are insulated in the presence of a horizontal plane air jet. Their results show that the heat exchange between the interior of the cavity and its surrounding can be avoided in the presence of an air jet with a high enough Reynolds number.

Vafai and Ettefagh [10] performed a study of buoyancy-driven flow with particular emphasis on the outer boundaries. A comprehensive investigation of the transient behavior of the flow and heat transfer characteristics inside and outside the cavity was presented in this work. The effects of the external corner on the flow and heat transfer and the influence of the far field boundary conditions on these quantities inside the open-ended cavity and its surrounding were explored in detail. Their results established that the extent of the outer boundaries had far more influence on the flow and temperature fields than that shown by other investigators. This work also illustrated in detail the effects of the Prandtl number, Rayleigh number, and the aspect ratio of the cavity on the heat transfer characteristics. The thermal

and fluid flow instabilities in buoyancy-driven flows in open-ended cavities were also studied by the same authors [11]. Their results illustrated that the oscillations of the Nusselt number and that of the central vortex inside the cavity have the same frequency, and that this frequency, is related to the Rayleigh number.

Ettefagh and Vafai [12] conducted a study of natural convection in open-ended cavities in the presence of a porous medium. The influence of the external corners on vorticity generation and flow instability augmentation were discussed. The outer boundaries were set far enough so that the flow field inside the cavity and that approaching the aperture plane were not influenced by the far field boundary conditions. The effect of pertinent parameters such as the Darcy-Rayleigh number, and aspect ratio among others were analyzed and discussed. Their results illustrated that decreasing the aspect ratio has a stabilizing effect on the flow field. Ettefagh et al. [13] conducted a study of non-Darcian effects in open-ended cavities filled with a porous medium. Several types of flow models such as Brinkman-extended Darcy, Forchheimer-extended Darcy, and the generalized flow models were analyzed in this work. The importance of the inertial and boundary effects and their crucial influence on the streamlines and isotherms in open-ended cavities was investigated.

Khanafer and Vafai [14] performed a study of buoyancy-driven flow and heat transfer in an open-ended cavity. To reduce the storage capacity and the computational time, effective boundary conditions were established to replace the extended boundaries. Both 2-D and 3-D geometries were analyzed in their work. The comparisons for the streamlines and isotherms between 2-D and 3-D models utilizing effective boundary conditions and the fully extended domain simulations displayed an excellent agreement. Later on, these authors [15] presented a study of buoyancy-driven flow and heat transfer in a 2-D open-ended enclosure for a wide range of pertinent parameters, such as Rayleigh and Prandtl numbers and the aspect ratio. They established that the effective boundaries are related to Rayleigh and Prandtl numbers and the aspect ratio. Comprehensive comparisons for the flow and temperature field inside the cavity were done for a wide range of parameters between the 2-D closed-ended model and the 2-D model utilizing the far field boundary conditions. An excellent agreement was found between the two models. Khanafer and Vafai have also presented a study of double-diffusive mixed convection in a lid-driven enclosure [16].

Khanafer et al. [17] performed a study of mixed convection heat transfer in 2-D open-ended cavities. Three different angles of attack (0°, 45°, and 90°) were analyzed in this work. A wide range of Grashof number from 10^2 to 10^5, Reynolds number from 10^2 to 10^4, and aspect ratio from 0.25 to 1 was investigated in this study. Their results show that at lower Grashof numbers the average Nusselt number increases almost linearly with the Reynolds number for different angles of attack. The flow field was shown to be dominated by the external flow beyond a critical Reynolds number. The effects of the aspect ratio were also investigated in this work, and it was shown that a decrease in the aspect ratio decreased the thickness of the thermal boundary layer along the lower and upper horizontal walls. This resulted in a heat transfer enhancement from both horizontal walls. More recent works on natural and mixed convection in cavities have been performed by Kumar et al. [18], Vishnuvardhanarao and Das [19], Basak et al. [20], Chen et al. [21], and Marcondes et al. [22].

The present work focuses on simulation of mixed convection in a two-dimensional open-ended cavity which is filled with a porous medium. Effects of

different pertinent controlling parameters such as Grashof, Reynolds, and Darcy numbers for different angles of attack (0°, 45°, and 90°) are investigated using a generalized flow model [23, 24]. A detailed analysis of the pertinent physical controlling parameters is done through synthesis of streamlines, isotherms, and Nusselt number distributions.

2. MODEL CONFIGURATION AND GOVERNING EQUATIONS

2.1. Physical Model and Assumptions

The configuration described in this investigation is shown in Figure 1*a*. The domain under consideration is based on a two-dimensional open-ended cavity of height H and width $2w$. L_x, L_y are the extended computational domain lengths in x- and y-directions, respectively. This model is similar to the configuration used by Khanafer et al. [17]. In this investigation, half of the open-ended cavity is considered based on symmetry considerations, as shown in Figure 1*b*. Air is utilized as the working fluid. The open-ended cavity with the extended computational domain is filled with a porous medium, which is isotropic and homogeneous.

The dimensionless governing equations for continuity, momentum, and energy conservation can be written as

$$\frac{\partial U}{\partial X}+\frac{\partial V}{\partial Y}=0 \tag{1}$$

$$\frac{1}{\delta}\left(\frac{\partial \overline{U}}{\partial \tau}+U\frac{\partial \overline{U}}{\partial X}+V\frac{\partial \overline{U}}{\partial Y}\right)=-\frac{1}{\mathrm{Re}}\nabla P+\frac{1}{\mathrm{Re}}\left(\frac{\partial^2 \overline{U}}{\partial X^2}+\frac{\partial^2 \overline{U}}{\partial Y^2}\right)+\frac{\mathrm{Gr}}{\mathrm{Re}^2}\theta j-\frac{1}{\mathrm{DaRe}}\overline{U}-F\delta \mathrm{Da}^{-\frac{1}{2}}(|\overline{U}|\overline{U}) \tag{2}$$

$$\frac{\partial \theta}{\partial \tau}+U\frac{\partial \theta}{\partial X}+V\frac{\partial \theta}{\partial Y}=\frac{1}{\mathrm{Re}\,\mathrm{Pr}}\left(\frac{\partial^2 \theta}{\partial X^2}+\frac{\partial^2 \theta}{\partial Y^2}\right) \tag{3}$$

where F is an inertial coefficient which depends on the Reynolds number and the micro-structure of the porous medium. The employed dimensionless variables used in the governing equations are

$$X=\frac{x}{H},\quad Y=\frac{y}{H},\quad U=\frac{u}{U_o},\quad V=\frac{v}{U_o},\quad \theta=\frac{T-T_\infty}{T_w-T_\infty},\quad P=\frac{p}{\rho U_o^2}$$
$$\mathrm{Gr}=\frac{g\beta H^3\Delta T}{\nu^2},\quad \mathrm{Pr}=\frac{\nu}{\alpha},\quad \mathrm{Da}=\frac{K}{H^2},\quad R_e=\frac{U_o H}{\nu},\quad \tau=\frac{U_o t}{H} \tag{4}$$

where Gr is the Grashof number, Pr is the Prandtl number, Da is the Darcy number, and Re is the Reynolds number.

2.2. Boundary Conditions

The boundary conditions for the computational domain for three different angles of attack (0°, 45°, and 90°) are shown in Figure 1. The temperature of the

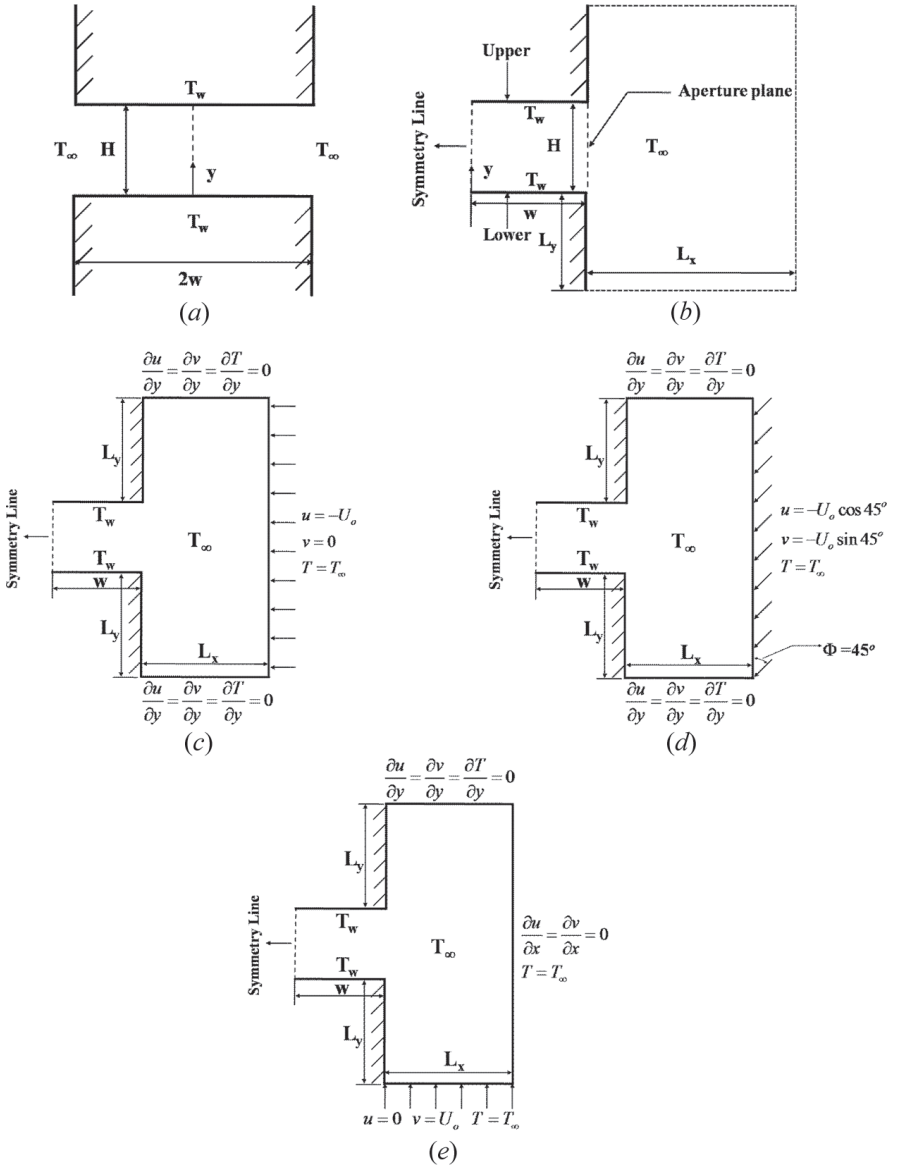

Figure 1. (*a*) Physical configuration and (*b*) extended physical configuration employing the symmetry condition; boundary conditions for (*c*) horizontal flow, (*d*) inclined flow, and (*e*) vertical flow.

upper and lower horizontal wall is fixed at T_w, which is higher than the ambient temperature T_∞. The vertical walls are assumed to be insulated. The extended computational domain boundary conditions are based on vanishing normal gradients for the temperature and the velocity.

3. NUMERICAL PROCEDURE

The commercial software COMSOL was utilized to solve the governing equations. Convergence was set at 10^{-6}. The present numerical scheme was validated against the numerical results obtained by Khanafer et al. [17], as shown in

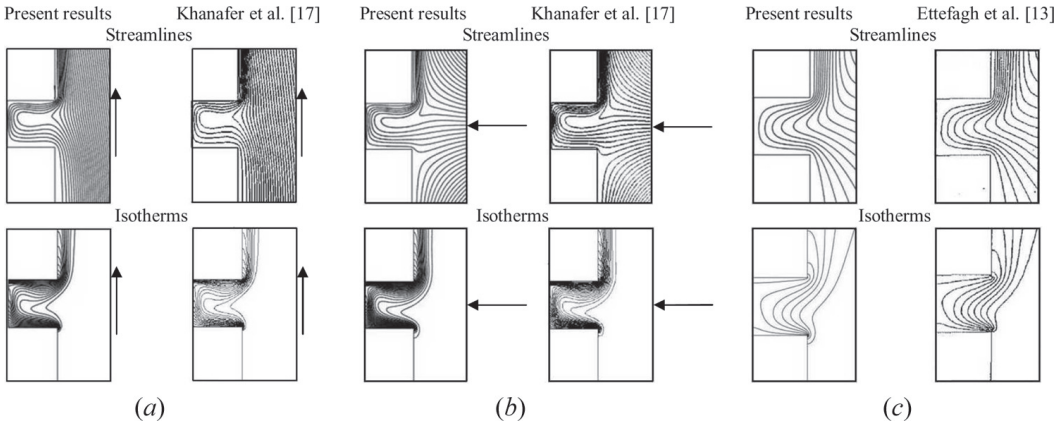

Figure 2. Comparison of streamlines and isotherms between the present numerical results and that of Khanafer et al. [17] for (*a*) vertical external flow with $\mathrm{Re} = 10^2$ and $\mathrm{Gr} = 10^5$; (*b*) horizontal external flow and $\mathrm{Re} = 10^2$ and $\mathrm{Gr} = 10^5$; (*c*) comparison of streamlines and isotherms between the present numerical results and that of Ettefagh et al. [13] for modified $\mathrm{Ra} = 10^2$, $\mathrm{Pr} = 1.0$, and $\mathrm{Da} = 10^{-2}$.

Figures 2*a* and 2*b*. As can be seen in these figures, there is excellent agreement between the present work and the results obtained by Khanafer et al. [17]. An additional comparison was also done with the results of Ettefagh et al. [13], as shown in Figure 2*c*. Once again, the results are in excellent agreement. A nonuniform distributed triangular mesh was employed in our computational simulations. The grid independence studies are shown in Figure 3 for three different mesh distributions shown in Table 1. Different cases analyzed in this study are shown in Table 2. The average Nusselt number along the upper and lower horizontal cavity walls is used as a yardstick for our grid independence study. As seen in Figure 3, the largest difference between mesh 1 and mesh 2 was less than 6%, and that between mesh 2

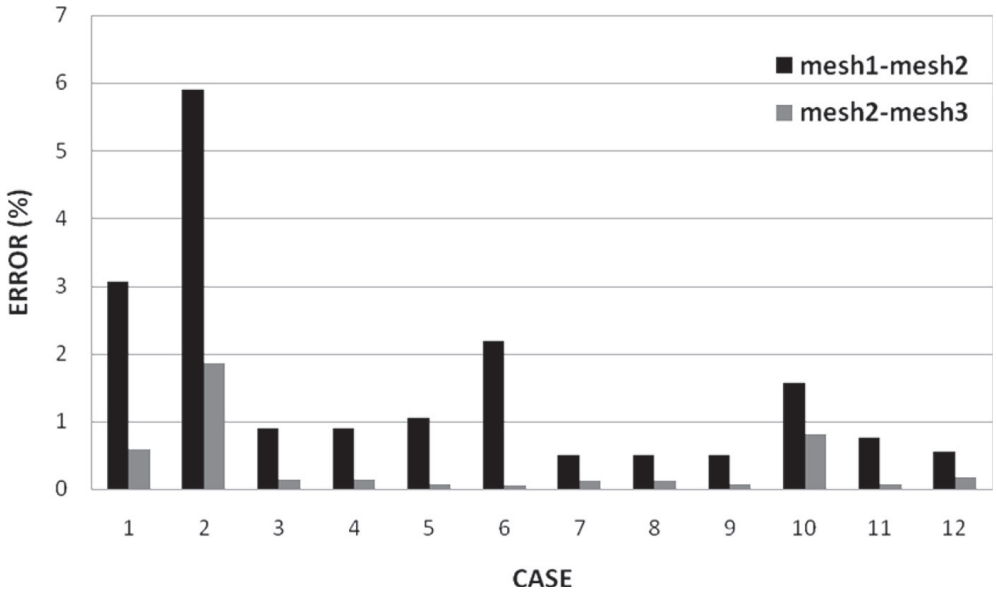

Figure 3. Comparisons between mesh 1 (coarser mesh), mesh 2 (finer mesh), and mesh 3 (finest mesh).

Table 1. Number of elements utilized in three different mesh distributions used in this work

	Mesh 1	Mesh 2	Mesh 3
Number of the elements	33,761	50,305	75,961

Table 2. Different cases analyzed in this work

Case	Re	Da	Gr	Φ
1	10^2	10^{-6}	10^{12}	0°
2	10^2	10^{-4}	10^{10}	0°
3	5×10^4	10^{-4}	10^2	0°
4	5×10^4	10^{-6}	10^2	0°
5	10^2	10^{-6}	10^{12}	90°
6	10^2	10^{-4}	10^{10}	90°
7	2×10^4	10^{-6}	10^2	90°
8	2×10^4	10^{-4}	10^2	90°
9	10^2	10^{-6}	10^{12}	45°
10	10^2	10^{-4}	10^{10}	45°
11	5×10^4	10^{-4}	10^2	45°
12	5×10^4	10^{-6}	10^2	45°

and mesh 3 was less than 1% except for case 2, which produced a difference less than 2%. As such, mesh 2 was selected for the results produced in this work.

4. RESULTS AND DISCUSSION

The governing equations are solved for a wide range of Reynolds, Darcy, and Grashof numbers and aspect ratios. The working fluid is chosen as air with a $\mathrm{Pr} = 0.71$. For each configuration, the Reynolds number is varied from 10^2 to 10^5, the Grashof number is varied from 10^2 to 10^9, the Darcy number variations is from 10^{-6} to 10^{-1}, and the aspect ratio variations is from 0.25 to 2.

4.1. Effect of the Grashof Number

The effect of the Grashof number on the streamlines for different external flow field angles of attack is presented in Figures 4–7 for a Darcy number of 10^{-4}. Figure 4 shows the effect of the Grashof number on the streamlines and isotherms for a horizontal angle of attack. Here, the Darcy and Reynolds numbers are set at $\mathrm{Da} = 10^{-4}$ and $\mathrm{Re} = 10^2$, while the Grashof number is varied from 10^4 to 10^9. It can be seen that at a low Grashof number (Figure 4*a*) the flow field shows a symmetry pattern with respect to the horizontal center line of the cavity. As the Grashof number increases (Figure 4*b*) the cold fluid is sucked into the cavity. As the Grashof number increases further (Figures 4*c* and 4*d*), the cold fluid penetrates further into the cavity. When the Grashof number approaches 10^8 (Figure 4*e*), the outside fluid reaches the corners of the cavity. This action is due to the buoyancy effect inside the cavity. Cold fluid is

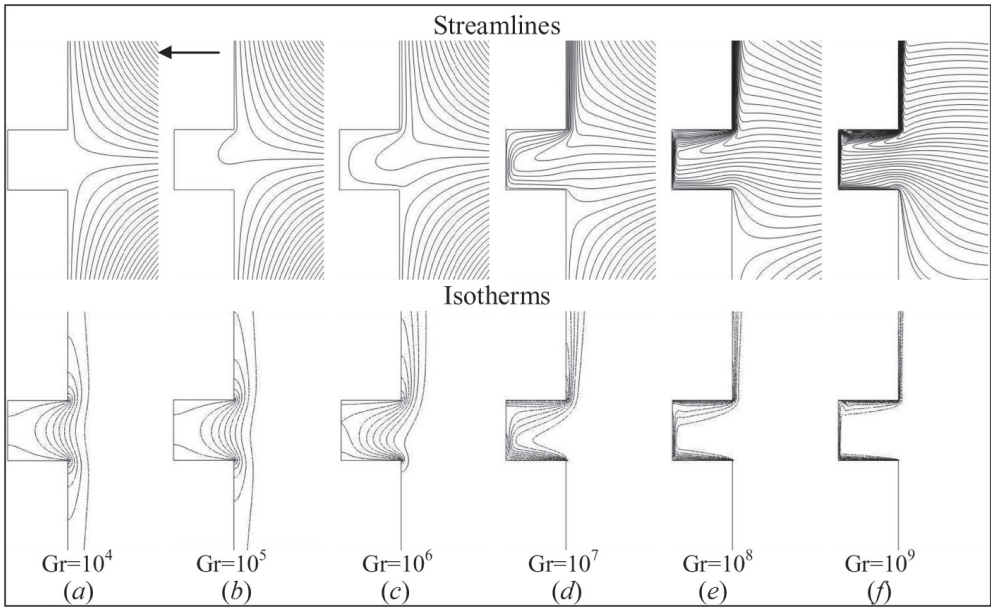

Figure 4. Effect of Grashof number on streamlines and isotherms for a horizontal external flow ($AR = 1$, $Re = 10^2$, and $Da = 10^{-2}$).

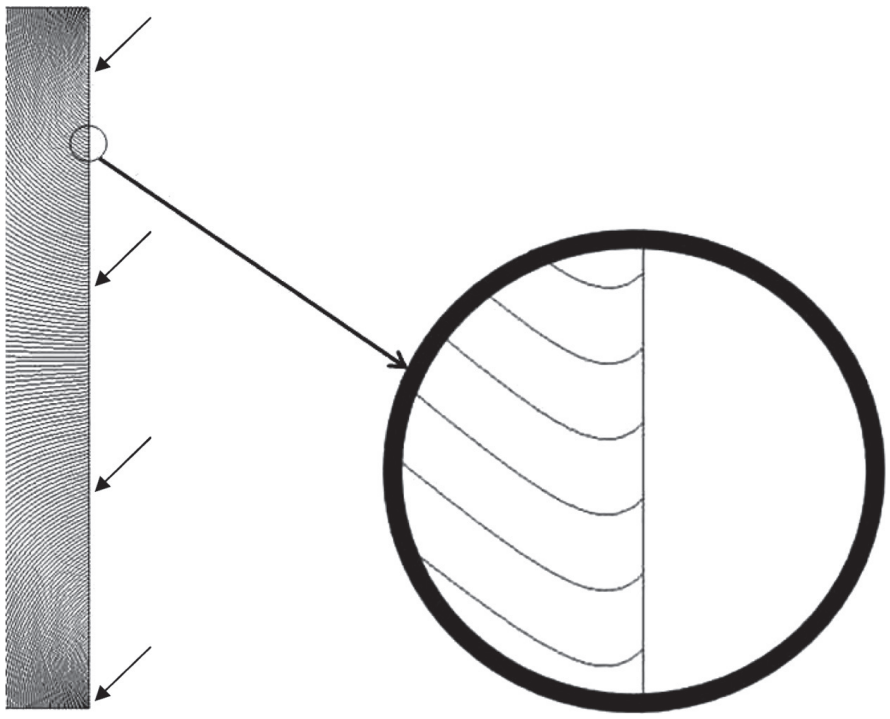

Figure 5. Flow behavior at the entrance boundary for a 45° external flow ($AR = 1$, $Gr = 100$, $Re = 2 \times 10^3$, and $Da = 10^{-2}$).

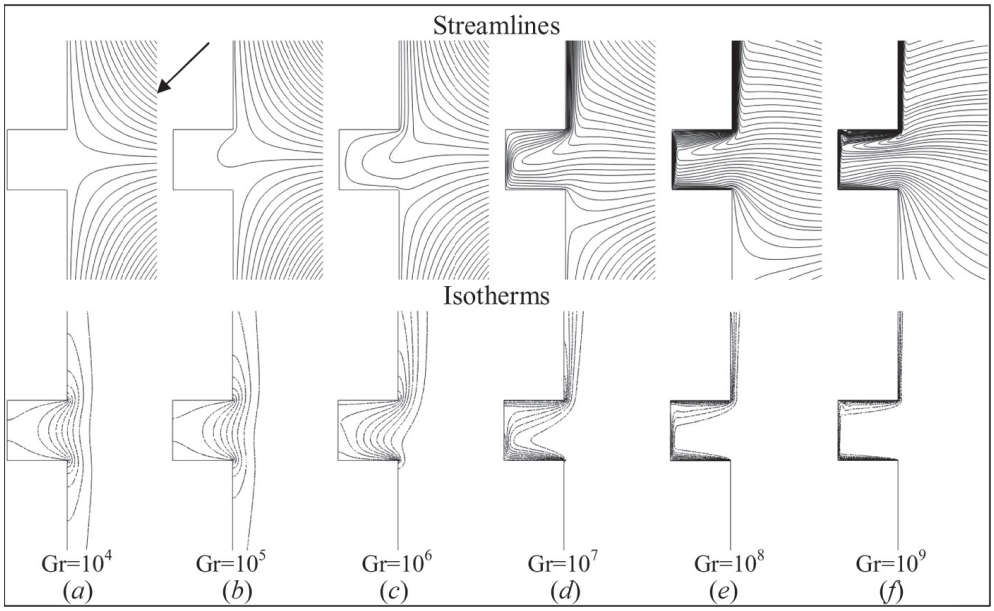

Figure 6. Effect of Grashof number on streamlines and isotherms for an inclined external flow (AR = 1, $Re = 10^2$, and $Da = 10^{-2}$).

heated by the lower horizontal wall; as a result, the heated fluid moves up and out of the cavity from the top part of the opening. Subsequently, cold fluid from the outside domain will be sucked into the cavity from the bottom portion of the opening to displace the ejected fluid. At higher Grashof numbers, the buoyancy effect is more

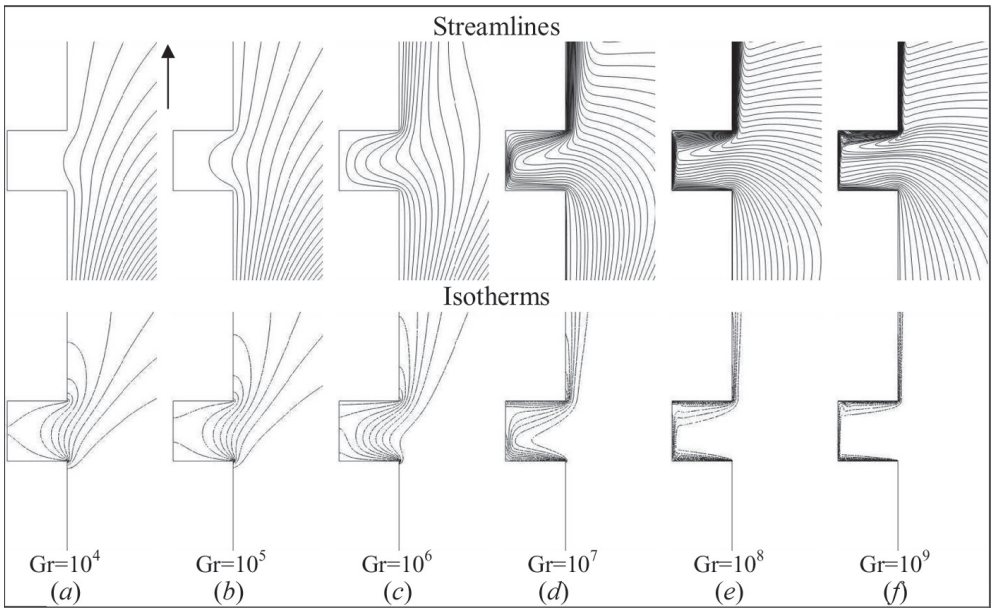

Figure 7. Effect of Grashof number on streamlines and isotherms for a vertical external flow (AR = 1, $Re = 10^2$, and $Da = 10^{-2}$).

pronounced, resulting in the ejected hot fluid to escape the cavity at a higher speed. Figures 4*e* and 4*f* display a substantial natural convection flow pattern along with the presence of a thin plume at the symmetry line.

Isotherms in Figure 4*a* show that the effect of external flow on the heat transfer inside the cavity is limited, and that conduction is the dominant mode of heat transfer. The external horizontal flow has a slight effect near the opening of the cavity. As the Grashof number increases, natural convection becomes more pronounced and the conduction-dominated heat transfer inside the open-ended cavity is replaced by convective heat transfer, as illustrated by the shape of the isotherms in Figure 4*c*. A further increase in the Grashof number contributes to a thinner thermal layer along the two horizontal walls, as well as a thinner boundary layer along the symmetry line, as seen in Figures 4*d*–4*f*.

Figure 5 shows that the influence from the vertical component of the external flow is quite limited and acts over a relatively narrow region. Beyond this region, the influence of the vertical component of the velocity greatly diminishes. It should be noted that this narrow region is further reduced for Darcy numbers which are lower than 10^{-2}. This behavior was also independently confirmed by using the Fluent commercial software. Results in Figure 6 show that an inclined external flow has similar flow and heat transfer behavior as a horizontal external flow. However, the inclined external flow diminishes the speed of the flow inside of the cavity at given Grashof and Reynolds numbers as compared to the case for the horizontal external flow.

Figure 7 shows the effect of the Grashof number on the streamlines and isotherms for a vertical external flow. In Figure 7, Darcy and Reynolds numbers are fixed at $\mathrm{Da} = 10^{-4}$ and $\mathrm{Re} = 10^2$, while the Grashof number is varied from 10^4 to 10^9. At low Grashof numbers, there is only a limited fluid penetration into the cavity and conduction is the dominant mode of energy transport. As the Grashof number increases, buoyancy becomes more dominant resulting in substantially more fluid penetration into the cavity (Figures 7*d*–7*f*), resulting in a substantial clustering of the isotherms near the symmetry line.

4.2. Effect of the Reynolds Number

4.2.1. Effect of the Reynolds number for low Grashof numbers. Effect of Reynolds number on the streamlines, isotherms, and the Nusselt number distributions for low Grashof number for three different angles of attack is presented in Figures 8–10 for $\mathrm{Da} = 10^{-6}$. Effect of Reynolds number on streamlines and isotherms for a horizontal angle of attack is displayed in Figure 8(I), where the Darcy and Grashof numbers are $\mathrm{Da} = 10^{-6}$ and $\mathrm{Gr} = 10^2$, while the Reynolds number is varied from 10^2 to 5×10^4. It can be seen from Figures 8*a*–8*e* that forced convection is the dominant flow mechanism, and that the streamlines show a symmetrical behavior about the horizontal centerline of the cavity. It can be seen in Figure 8*a* that the effect of external flow and buoyancy on heat transfer inside the cavity can be neglected, and that conduction is the dominant mode of heat transfer. As the Reynolds number increases, forced convection becomes dominant as evidenced by the isotherms. As the Reynolds number increases further (Figure 8*e*), isotherms along the horizontal walls are compressed further leading to a thinner thermal layer which increases the heat transfer effectiveness inside the open cavity.

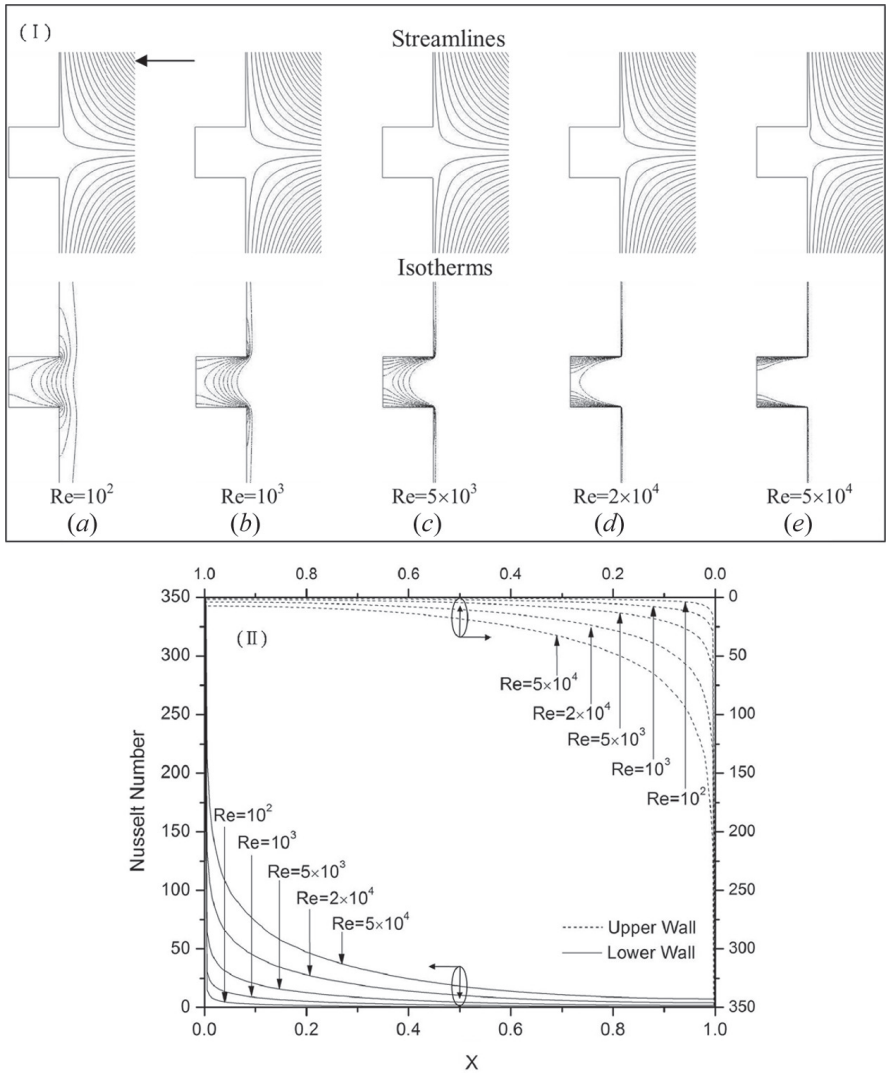

Figure 8. Effect of Reynolds number for a horizontal external flow ($AR = 1$, $Gr = 10^2$, and $Da = 10^{-6}$). (I) Streamlines and isotherms, and (II) Nusselt number distribution at lower and upper horizontal walls.

Figure 8(II) shows the Nusselt number distribution at the lower and upper horizontal walls for different Reynolds numbers. Variations of the Nusselt number along both the upper and lower walls for different Reynolds numbers show the same trend. As expected, the Nusselt number has a maximum value at the entrance of the cavity which subsequently decreases along the cavity. It can be seen that close to the symmetry line, the Nusselt number is almost constant. As expected, the Nusselt number increases as the Reynolds number increases.

Figure 9(I) shows that an inclined external flow has a similar flow structure and heat transfer characteristics as a horizontal external flow. However, through careful observation of the isotherms, it can be seen that the strength of the external flow has diminished for this case as compared to the horizontal external flow. This is due to the effective loss of the vertical component of the velocity at the

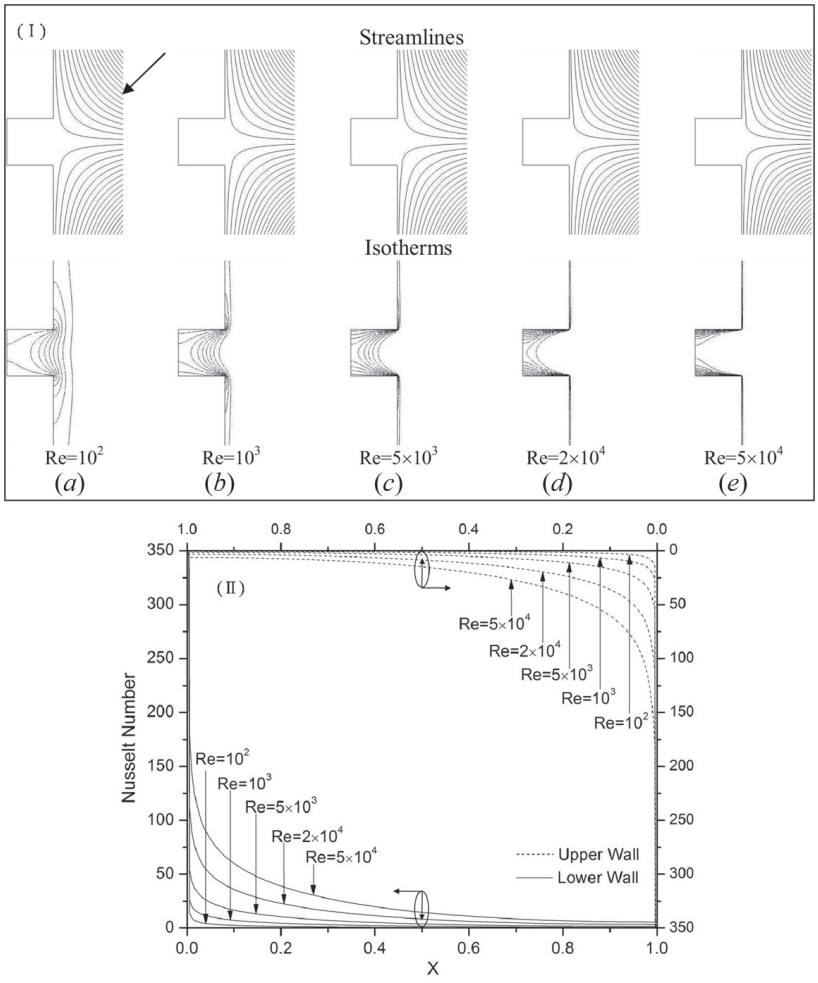

Figure 9. Effect of Reynolds number for an inclined external flow ($AR = 1$, $Gr = 10^2$, and $Da = 10^{-6}$). (I) Streamlines and isotherms, and (II) Nusselt number distribution at lower and upper horizontal walls.

inlet boundary. The effect of the Reynolds number on the Nusselt number distribution at the lower and upper horizontal walls for an inclined external flow is illustrated in Fig. 9(II). As discussed earlier, the Nusselt number distribution along the walls for an inclined external flow displays the same trend as that for the horizontal flow. However, since the vertical component of the velocity is diminished at the inlet boundary, at a given Reynolds number and location the Nusselt number for an inclined external flow is slightly less than that for horizontal external flow.

Figure 10(I) illustrates the effect of Reynolds number on the streamlines and isotherms for a vertical external flow. It can be seen that even though the speed of external flow increases with an increase in the Reynolds number, the flow pattern is not substantially affected by different Reynolds numbers. Isotherms in Figure 10*a* confirm that the heat transfer inside the open cavity is dominated by conduction due to the low Grashof and Reynolds numbers. The external flow has

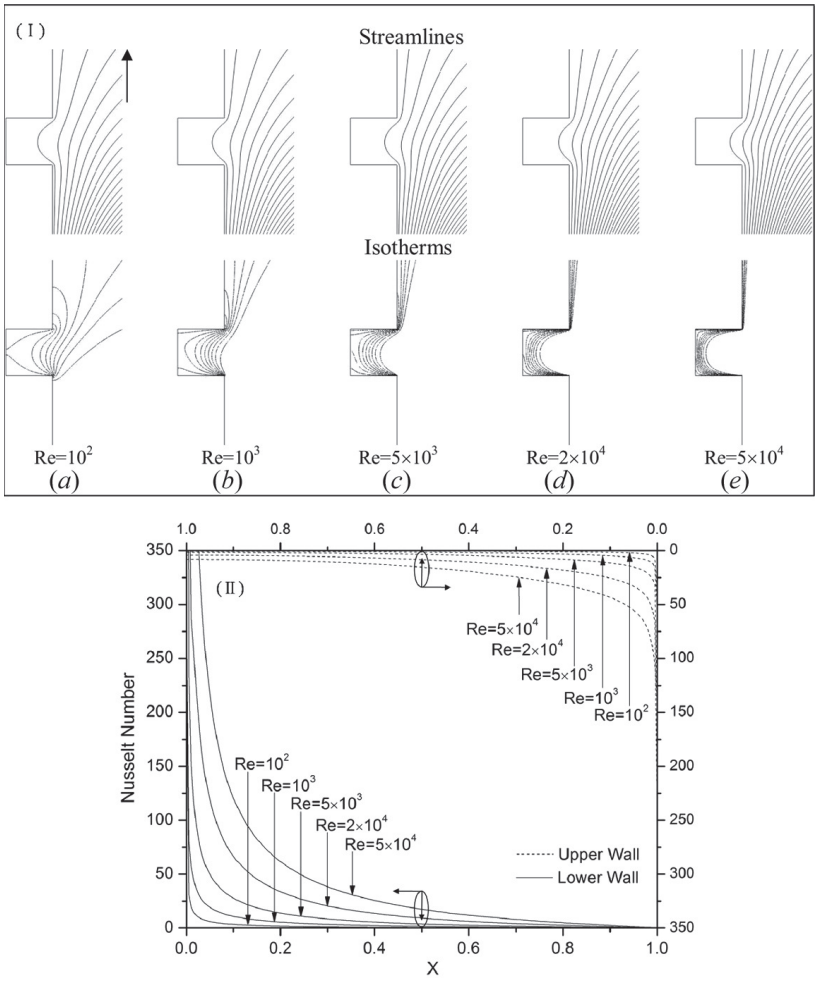

Figure 10. Effect of Reynolds number for a vertical external flow ($AR = 1$, $Gr = 10^2$, and $Da = 10^{-6}$). (I) Streamlines and isotherms, and (II) Nusselt number distribution at lower and upper horizontal walls.

a limited impact inside the cavity. As the Reynolds number increases (Figures 10*b* and 10*c*), forced convection is enhanced resulting in a compression of the isotherms inside the open cavity. As the Reynolds number increases further (Figures 10*d* and 10*e*), the effect of external flow becomes more significant leading to further compression of isotherms, and higher heat transfer rates through the upper and lower horizontal walls, as seen in Figure 10.

Figure 10(II) shows the effect of the Reynolds number on the Nusselt numbers at the lower and upper walls for a vertical external flow. It can be seen that the symmetrical characteristics which were present for a horizontal external flow is absent for a vertical external flow. Within the entrance section, the Nusselt number at the lower horizontal wall is substantially higher than that of upper wall. However, beyond $X = 0.6$, the Nusselt number at the upper wall becomes slightly larger due to the suction and ejection interactions with the external flow at the lower and upper boundaries, respectively.

4.2.2. Effect of Reynolds number for high Grashof numbers. The effect of Reynolds number on the streamlines, isotherms, and the Nusselt number distributions for high Grashof numbers for different types of external flow is illustrated in Figures 11–13, where the Darcy number is fixed at 10^{-6}. Figure 11(I) presents the effect Reynolds number for a horizontal external flow for a high Grashof number ($\mathrm{Gr} = 10^8$). The buoyancy forces are dominant within the cavity, as seen by the displayed flow structure in Figure 11*a*. As the Reynolds number increases, the external flow starts to have a more prominent effect on the flow pattern, resulting in a reduction of the penetration into the cavity. As seen in Figure 11*b*, the interaction between the external forced convection and the internal buoyancy driven convection determines the flow and temperature fields. Beyond $\mathrm{Re} = 2 \times 10^4$, the external flow becomes dominant resulting in a symmetrical flow pattern.

Figure 11(II) shows the effect of Reynolds number on the Nusselt number distribution at the lower and upper walls for a horizontal external flow for a high

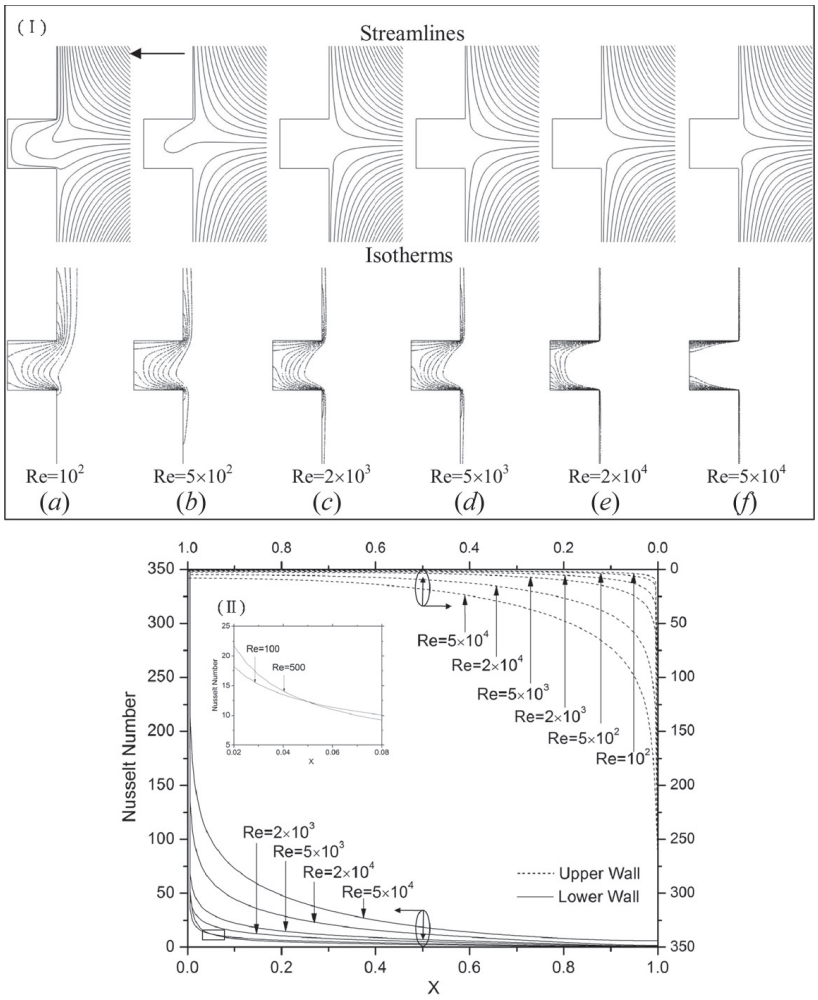

Figure 11. Effect of Reynolds number for a horizontal external flow ($\mathrm{AR} = 1$, $\mathrm{Gr} = 10^8$, and $\mathrm{Da} = 10^{-6}$). (I) Streamlines and isotherms, and (II) Nusselt number distribution at lower and upper horizontal walls.

Grashof number. It can be seen that the Nusselt number distribution in this case is similar to previous cases. One difference is in terms of the crossover that occurs for Reynolds numbers of 100 and 500. Up until $X = 0.05$, as expected, the Nusselt number for $\mathrm{Re} = 500$ is greater than that for $\mathrm{Re} = 100$. However, after $X = 0.05$ there is a crossover and the Nusselt number for $\mathrm{Re} = 100$ becomes larger than that for $\mathrm{Re} = 500$. The reason for this is due to the competing effects of natural and forced convection inside the cavity. It should be noted that the external flow can disturb the natural convection over part of the cavity.

Figure 12 shows the effect of the Reynolds number on streamlines, isotherms, and the Nusselt number distribution for an inclined flow for $\mathrm{Gr} = 10^8$. As can be seen, the flow and isotherm patterns and the Nusselt number distribution are similar to that for the horizontal external flow shown in Figure 11. Figure 13 shows the effect of the Reynolds number on streamlines, isotherms, and the Nusselt number distribution for a vertical external flow for $\mathrm{Gr} = 10^8$. As was the case for the horizontal and inclined external flows, natural convection is dominant inside of the cavity at

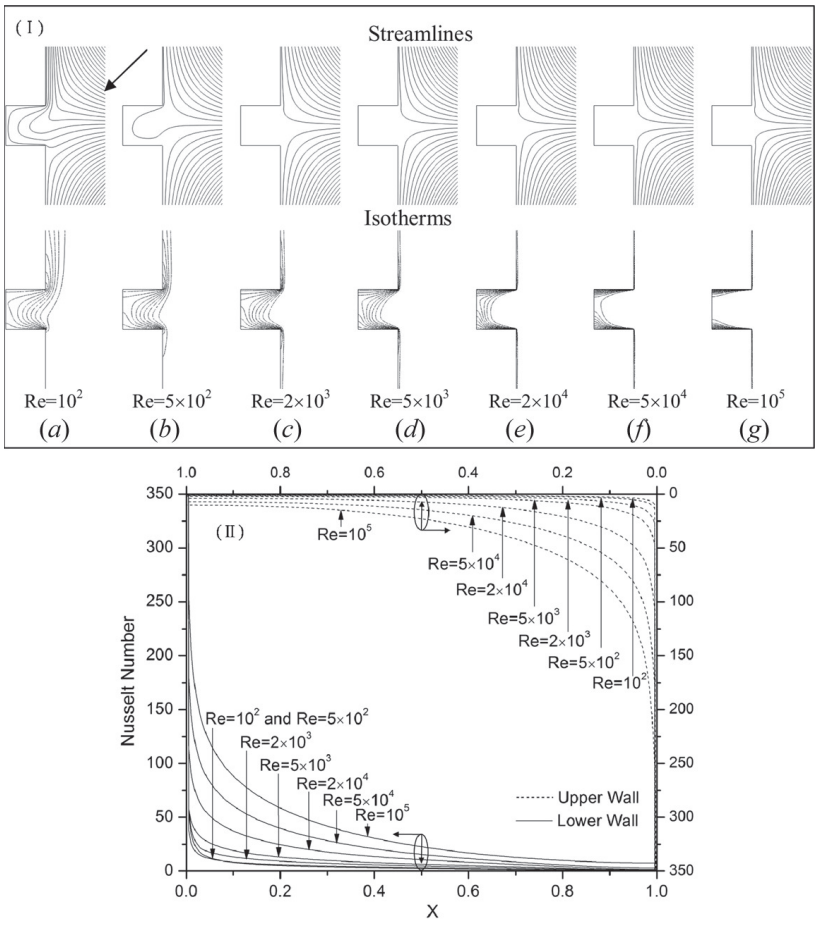

Figure 12. Effect of Reynolds number for an inclined external flow ($\mathrm{AR} = 1$, $\mathrm{Gr} = 10^8$, and $\mathrm{Da} = 10^{-6}$). (I) Streamlines and isotherms, and (II) Nusselt number distribution at lower and upper horizontal walls.

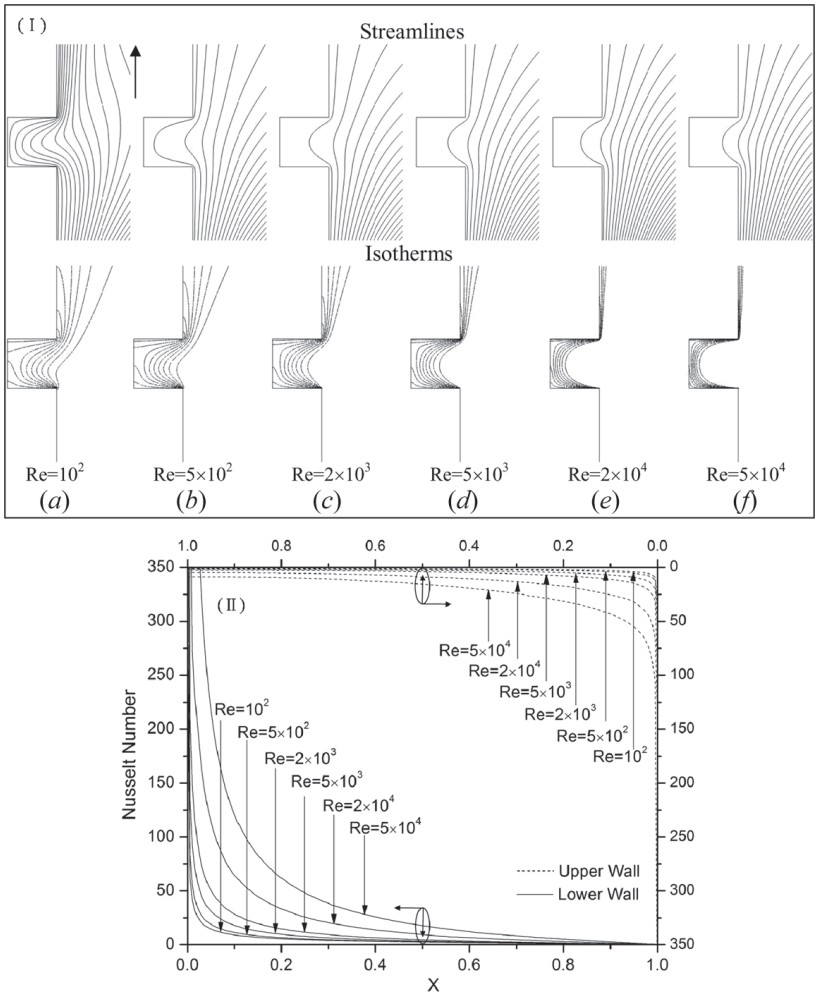

Figure 13. Effect of Reynolds number for a vertical external flow ($AR = 1$, $Gr = 10^8$, and $Da = 10^{-6}$). (I) Streamlines and isotherms, and (II) Nusselt number distribution at lower and upper horizontal walls.

low Reynolds numbers while the external flow becomes more dominant as the Reynolds number increases. The Nusselt number distribution in this case, shown in Figure 13(II), is similar to that for low Grashof numbers shown in Figure 10(II), with the Nusselt number at the lower wall being substantially higher than that for the upper wall.

4.3. Effect of the Darcy Number

Figures 14–16 illustrate the effect of the Darcy number on the streamlines, isotherms, and the Nusselt number distributions for different flow configurations. Darcy number varies from 10^{-6} to 10^{-1} while the Grashof and Reynolds numbers are fixed at 10^6 and 10^2, respectively.

Figure 14 displays the effect of the Darcy number for a horizontal external flow. The fluid cannot penetrate into the cavity due to the relatively low permeability

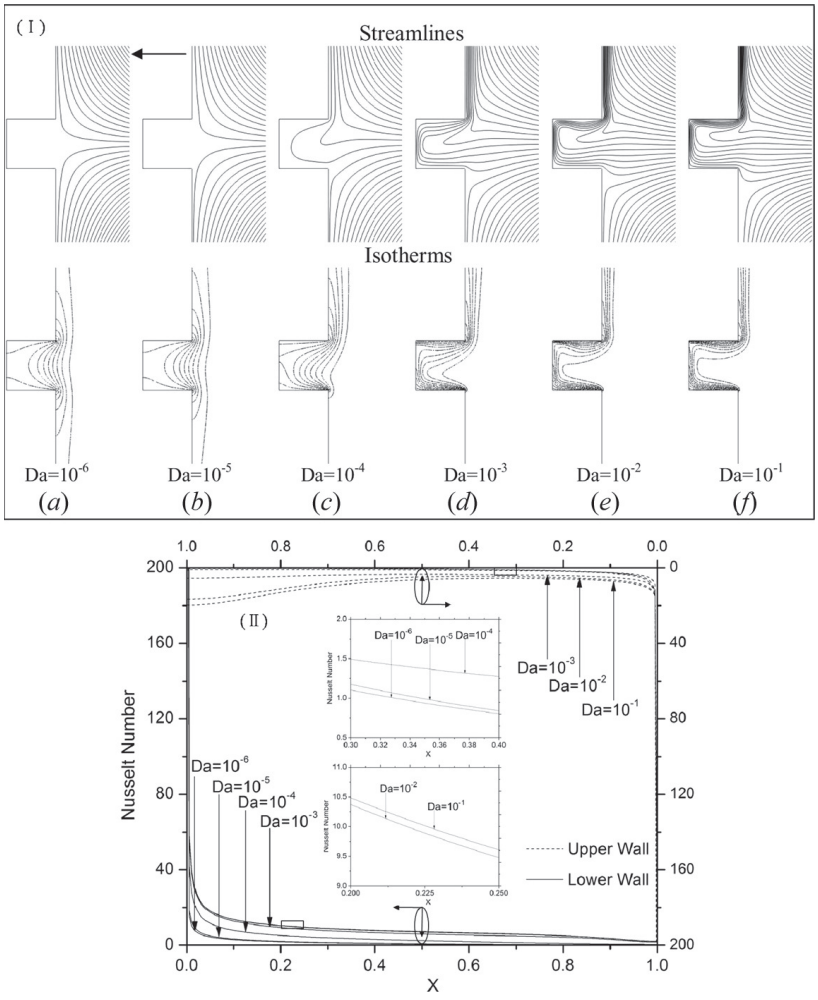

Figure 14. Effect of Darcy number for a horizontal external flow ($AR = 1$, $Gr = 10^6$, and $Re = 10^2$). (I) Streamlines and isotherms, and (II) Nusselt number distribution at lower and upper horizontal walls.

of the porous medium for low Reynolds number when $Da = 10^{-6}$, as seen in Figure 14*a*. As the Darcy number increases (Figure 14*c*), the porous medium becomes more permeable, resulting in a better penetration of the external flow into the cavity. As the Darcy number increases further (Figures 14*d* and 14*e*), there is additional penetration into the cavity. Isotherms in Figures 14*a* and 14*b* indicate that conduction is the dominant mode of heat transfer inside the cavity for $Da < 10^{-5}$. The buoyancy effect becomes more prominent as the Darcy number increases (Figure 14*c*). As the Darcy number increases further, natural convection becomes dominant. A similar trend is observed for an inclined external flow, which is shown in Figure 15.

For a vertical external flow, Figure 16 displays similar characteristics as prior configurations. Figures 14(II), 15(II), and 16(II) show the effect of the Darcy number on the Nusselt number distribution at lower and upper horizontal walls for three different flow configurations. It is seen that as the Darcy number increases, the Nusselt

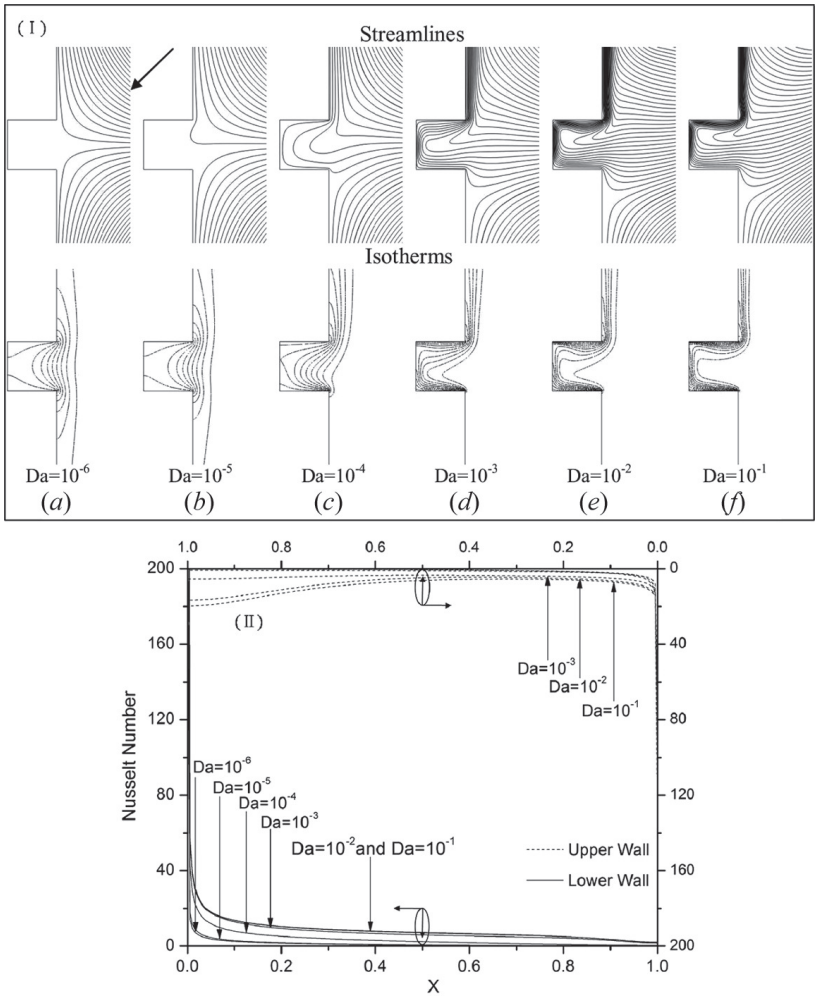

Figure 15. Effect of Darcy number for an inclined external flow ($AR = 1$, $Gr = 10^6$, and $Re = 10^2$). (I) Streamlines and isotherms, and (II) Nusselt number distribution at lower and upper horizontal walls.

number at the lower and upper wall increases resulting in higher heat transfer rates along the horizontal walls.

4.4. Effect of Aspect Ratio

The effect of the aspect ratio on the streamlines and isotherms for a horizontal external flow is displayed in Figures 17*a*–17*d* for $Da = 10^{-6}$, $Gr = 10^9$, and $Re = 10^2$. It can be seen that the flow structure outside the cavity is stable for different aspect ratios. It is shown that the fluid can still reach the symmetry line of the cavity even as the cavity becomes deeper at large aspect ratios. Isotherm pattern in Figures 17*a*–17*d* shows that as the aspect ratio increases, the thermal boundary layer becomes thicker, resulting in a lower heat transfer rate through the horizontal walls.

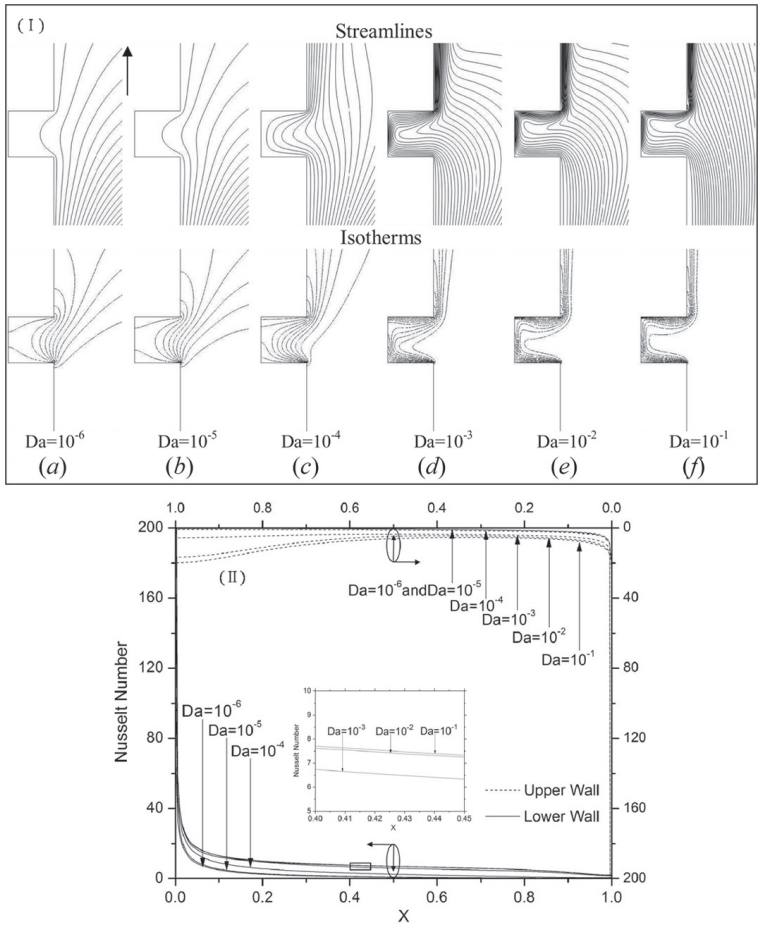

Figure 16. Effect of Darcy number for a vertical external flow ($AR = 1$, $Gr = 10^6$, and $Re = 10^2$). (I) Streamlines and isotherms, and (II) Nusselt number distribution at lower and upper horizontal walls.

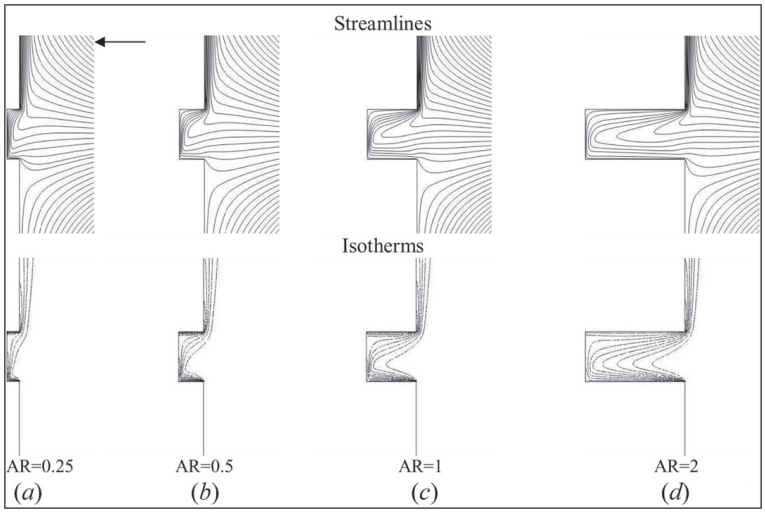

Figure 17. Effect of aspect ratio on streamlines and isotherms for a horizontal external flow ($Da = 10^{-6}$, $Gr = 10^9$, and $Re = 10^2$).

5. CONCLUSION

A numerical investigation of mixed convection in an obstructed two-dimensional open-ended cavity is presented. Effects of Grashof, Reynolds, and Darcy numbers and the aspect ratio on the flow and the temperature field are investigated in this study. As the Grashof number increases, the effect of buoyancy increases leading to a thinner thermal boundary layer along upper and lower horizontal walls, resulting in an enhanced heat transfer between the cavity and its surrounding. For low Grashof numbers, the external flow dominates the flow and heat transfer characteristics when Re is around 2×10^4 or larger, while for high Grashof numbers this domination occurs as Re increases to 10^5 for horizontal and inclined external flows. The vertical external flow cannot fully dominate the flow and heat transfer characteristics inside the open-ended cavity since the buoyancy force remains relatively strong. An increase in the Darcy number results in an increase in the fluid penetration and higher heat transfer inside the open-ended cavity. In addition, an increase in the aspect ratio is characterized by an increase in thickness of the thermal boundary layer which leads to a lower heat transfer rate through horizontal walls. Details of these cases were analyzed in depth and presented in terms of streamlines and isotherms, as well as the Nusselt number distributions along the upper and lower horizontal walls. The presented Nusselt number distributions further clarify the effects of pertinent physical parameters on mixed convection in an obstructed open-ended cavity.

REFERENCES

1. M. L. Doria, A Numerical Model for the Prediction of Two-Dimensional Unsteady Flows of Multi-Component Gases with Strong Buoyancy Effects and Recirculation, *Notre Dame Report*, TR-37191-74–4, 1974.
2. H. R. Jacobs, W. E. Mason, and W. T. Hikida, Natural Convection in Open Rectangular Cavities, In *Proc. Fifth Int. Heat Transfer Conf.*, Tokyo, Japan, vol. 3, pp. 90–94, 1974.
3. H. R. Jacobs and W. E. Mason, Natural Convection in Open Rectangular Cavities with Adiabatic Sidewalls, In *Proc. 1976 Heat Transfer and Fluid Mech. Inst.*, Stanford University Press, Stanford, pp. 33–46, 1976.
4. F. Penot, Numerical Calculation of Two-Dimensional Natural Convection in Isothermal Open Cavities, *Numer. Heat Transfer, Part A*, vol. 5, pp. 421–437, 1982.
5. O. LeQuere, J. A. C. Humphery, and F. S. Sherman, Numerical Calculation of Thermally Driven Two-Dimensional Unsteady Laminar Flow in Cavities of Rectangular Cross Section, *Numer. Heat Transfer, Part A*, vol. 4, pp. 249–283, 1981.
6. Y. L. Chan and C. L. Tien, A Numerical Study of Two-Dimensional Natural Convection in Square Open Cavities, *Numer. Heat Transfer, Part A*, vol. 8, pp. 65–80, 1985.
7. Y. L. Chan and C. L. Tien, A Numerical Study of Two-Dimensional Laminar Natural Convection in Shallow Open Cavities, *Int. J. Heat Mass Transfer*, vol. 28, pp. 603–612, 1985.
8. H. Mhiri, S. El Golli, A. Berthon, G. Le Palec, and P. Bournot, Numerical Study of the Thermal and Aerodynamic Insulation of a Cavity with a Vertical Downstream Air Jet, *Int. Comm. Heat Mass Transfer*, vol. 25, pp. 919–928, 1998.
9. S. Besbes, H. Mhiri, S. El Golli, G. Le Palec, and P. Bournot, Numerical Study of a Heated Cavity Insulated by a Horizontal Laminar Jet, *Energy Conv. Man.*, vol. 42, pp. 1417–1435, 2001.

10. K. Vafai and J. Ettefagh, The Effects of Sharp Corners on Buoyancy-Driven Flows with Particular Emphasis on Outer Boundaries, *Int. J. Heat Mass Transfer*, vol. 33, pp. 2311–2328, 1990.
11. K. Vafai and J. Ettefagh, Thermal and Fluid Flow Instabilities in Buoyancy-Driven Flows in Open-Ended Cavities, *Int. J. Heat Mass Transfer*, vol. 33, pp. 2329–2344, 1990.
12. J. Ettefagh and K. Vafai, Natural Convection in Open-Ended Cavities with a Porous Obstructing Medium, *Int. J. Heat Mass Transfer*, vol. 31, pp. 673–693, 1988.
13. J. Ettefagh, K. Vafai, and S. J. Kim, Non-Darcian Effects in Open-Ended Cavities Filled with a Porous Medium, *ASME J. Heat Transfer*, vol. 113, pp. 747–756, 1991.
14. K. Khanafer and K. Vafai, Buoyancy-Driven Flows and Heat Transfer in Open-Ended Enclosures: Elimination of the Extended Boundaries, *Int. J. Heat Mass Transfer*, vol. 43, pp. 4087–4100, 2000.
15. K. Khanafer and K. Vafai, Effective Boundary Conditions for Buoyancy-Driven Flows and Heat Transfer in Fully Open-Ended Two-Dimensional Enclosures, *Int. J. Heat Mass Transfer*, vol. 45, pp. 2527–2538, 2002.
16. K. Khanafer and K. Vafai, Double-Diffusive Mixed Convection in a Lid-Driven Enclosure Filled with a Fluid-Saturated Porous Medium, *Numer. Heat Transfer A*, vol. 42, pp. 465–486, 2002.
17. K. Khanafer, K. Vafai, and M. Lightstone, Mixed Convection Heat Transfer in Two-Dimensional Open-Ended Enclosure, *Int. J. Heat Mass Transfer*, vol. 45, pp. 5171–5190, 2002.
18. D. S. Kumar, A. K. Dass, and A. Dewan, Analysis of Non-Darcy Models for Mixed Convection in a Porous Cavity using a Multigrid Approach, *Numer. Heat Transfer A*, vol. 56, pp. 685–708, 2009.
19. E. Vishnuvardhanarao and M. K. Das, Laminar Mixed Convection in a Parallel Two-Sided Lid-Driven Differentially Heated Square Cavity Filled with a Fluid-Saturated Porous Medium, *Numer. Heat Transfer A*, vol. 53, pp. 88–110, 2008.
20. T. Basak, S. Roy, and H. S. Takhar, Effects of Nonuniformly Heated Wall(s) on a Natural-Convection Flow in a Square Cavity Filled with a Porous Medium, *Numer. Heat Transfer A*, vol. 51, pp. 959–978, 2007.
21. X. B. Chen, P. Yu, S. H. Winoto, and H. T. Low, Free Convection in a Porous Wavy Cavity Based on the Darcy-Brinkman-Forchheimer Extended Model, *Numer. Heat Transfer A*, vol. 52, pp. 377–397, 2007.
22. F. Marcondes, J. M. De Medeiros, and J. M. Gurgel, Numerical Analysis of Natural Convection in Cavities with Variable Porosity, *Numer. Heat Transfer A*, vol. 40, pp. 403–420.
23. K. Vafai, Convective Flow and Heat Transfer in Variable Porosity Media, *J. Fluid Mech.*, vol. 147, pp. 233–259, 1984.
24. K. Vafai, *Handbook of Porous Media*, 2nd ed., Marcel Dekker, New York, 2005.